

Electrical image potential and solvation energies for an ion in a pore in a metallic electrode or in a nanotube

J. B. Sokoloff 

*Physics Department, Northeastern University, Boston, Massachusetts 02115, USA
and Physics Department, Florida Atlantic University, Boca Raton, Florida 33431, USA*



(Received 24 December 2021; accepted 31 March 2022; published 18 April 2022)

Electrical image potentials can be important in small spaces, such as nanoscale pores in porous electrodes, which are used in capacitive desalination and in supercapacitors, as argued by Bazant's group at Massachusetts Institute of Technology. It will be shown here that inside pores in porous metallic materials the image potentials can be considerably larger than near flat walls, as a result of the fact that the dielectric constant for an electric field perpendicular to a wall is much smaller than the bulk dielectric constant of water. Calculations will be presented for the image potential in spherical and cylindrically shaped pores. The calculations for cylindrical pores can also be applied to nanotubes. It was believed for a long time, on the basis of molecular dynamics simulations, that in order to push a salt solution through a small radius nanotube, work must be done against the solvation energy of the ions, which is larger inside a narrow nanotube than it is in the bulk. The relatively large image charge potential energy in narrow nanotubes, however, tends to oppose this increase in the solvation energy. The degree to which the image potential facilitates the flow of the salt ions into nanotubes will be discussed.

DOI: [10.1103/PhysRevE.105.044606](https://doi.org/10.1103/PhysRevE.105.044606)

I. INTRODUCTION

Porous electrodes play an essential role in capacitive desalination [1–8] and supercapacitors [9–13]. In order to determine the ability of a porous material to absorb ions from a solution, it is essential to understand the various contributions to the energy of the ions in nanometer-scale pores. It was pointed out in Ref. [4] that the electrical image potential energy (i.e., the interaction of an ion with charge that it induces in the walls of a pore) makes an important contribution to the energy of the ions in the pores. (A more extended discussion of the relationship between the work reported in this paper and the fit to experimental data given in Ref. [4] will be given in Sec. V). Reference [4] and this work consider nanometer-scale pores in porous electrodes used in capacitive desalination and in supercapacitors, which are illustrated schematically in Fig. 1.

The nanopores can have arbitrary shapes. They can be compact or extended. To study these two possibilities, two pore shapes that can be easily treated mathematically will be considered here, a sphere and a cylinder. The electrical image potential energy also makes an important contribution to the energy of ions in nanotubes. In particular, they are able to make up for the loss of solvation energy when an ionic solution enters a nanotube, making it possible for ions to flow into even relatively narrow nanotubes. Here, the electrical image potential and solvation energy of ions within a spherically shaped and cylindrically shaped pore will be studied.

II. SPHERICAL PORES

First, let us consider, as a model for an ion, a spherical shell of radius a with a uniform charge q on its surface at the center of a spherical pore of radius b in a metallic electrode.

The image is a charged spherical shell of radius R , as illustrated in Fig. 2.

The permittivity inside the pore is likely a tensor, which when diagonalized has an r - r diagonal element equal to ϵ_{perp} which is considerably smaller than the permittivity in bulk water. For the case of an ion at the center of the pore, the electrical potential V satisfies Poisson's equation:

$$\epsilon_{\text{perp}} \frac{1}{r^2} \frac{d}{dr} \left(r^2 \frac{dV}{dr} \right) = 0. \quad (1)$$

The image charge, equal to $-q(a/r)$, is distributed uniformly over the image sphere. Then, the total potential at a distance r from the center of the pore is given in MKS units by

$$V = \frac{q}{4\pi\epsilon_{\text{perp}}r} - \frac{b}{r} \frac{q}{4\pi\epsilon_{\text{perp}}(b^2/r)} = \frac{q}{4\pi\epsilon_{\text{perp}}r} - \frac{q}{4\pi\epsilon_{\text{perp}}b}. \quad (2)$$

Consequently, the electrical image potential energy of the ion is given by

$$U_{\text{image}} = -\frac{q^2}{4\pi\epsilon_{\text{perp}}b} = -\frac{2\epsilon_{\parallel}}{\epsilon_{\text{perp}}} \frac{a}{b} \frac{q^2}{8\pi\epsilon_{\parallel}a}, \quad (3)$$

where ϵ_{\parallel} is the permittivity parallel to the pore's wall, since the second term in Eq. (2) is the potential due to the charge induced in the walls of the pore. Its interaction with the charge q is the image potential energy. The permittivity for fields normal to the pore wall ϵ_{perp} is $2.1\epsilon_0$ [14] (assuming that ϵ_{perp} for a curved surface is comparable to its value for a flat surface), where ϵ_0 is the permittivity of free space. The permittivity assumed in Ref. [4] was a scalar of magnitude between $8\epsilon_0$ and $16\epsilon_0$. Therefore, the image potential energy

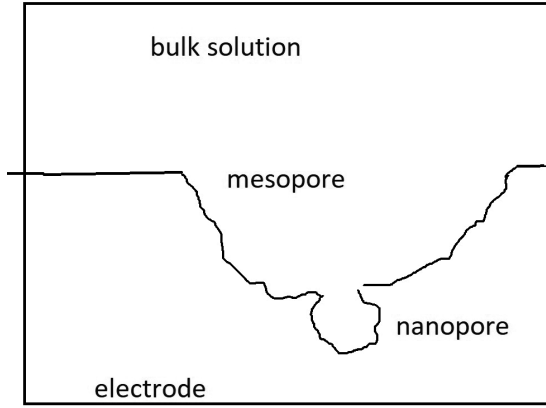


FIG. 1. A nanopore in a porous electrode is illustrated in this figure. As shown, the nanopore is generally connected to a mesoscopic pore.

for an ion at the center of a pore, given by Eq. (3), with b of the order of a nanometer is larger than the estimate in Ref. [4].

The image potential which lowers the energy of an ion when it is inside the pore is opposed by the self-energy, which is larger inside the pore than in the bulk fluid. In order to calculate the self-energy at the center of the pore, we use the electric field due to a charged spherical shell of radius a at the center of the pore, as a model for the ion, without the contribution from the charge rearrangement on the boundary of the pore needed to satisfy the boundary conditions [15]. It is given by

$$E = \frac{q}{4\pi\epsilon_{\text{perp}}r}. \quad (4)$$

The Born self-energy [16] is then given by

$$U = (1/2)\epsilon_{\text{perp}}(4\pi) \int_a^\infty r^2 dr E^2 = \frac{q^2}{8\pi\epsilon_{\text{perp}}a} \\ = \frac{\epsilon_{\parallel}}{\epsilon_{\text{perp}}} \frac{q^2}{8\pi\epsilon_{\parallel}a}. \quad (5)$$

U is independent of b . This likely occurs because U only depends on the form of the tensor permittivity, which has been assumed to have the form that was used to calculate U above no matter how large we choose b to be. In reality, however, if the radius is large enough (greater than 0.75 nm), the permittivity at the center of the tube will revert to its bulk water value [14]. If $\epsilon_{\parallel} = \epsilon = 81\epsilon_0$, $\epsilon_{\text{perp}} = 2.1\epsilon_0$ [14], where ϵ_{\parallel} is the permittivity component parallel to the wall of the pore, assumed to be comparable to the permittivity of the bulk fluid ϵ , we find from Eqs. (3) and (5) that $U_{\text{image}}/U = 2a/b$ at the center of the pore. U inside the pore is a factor $\epsilon_{\parallel}/\epsilon_{\text{perp}} = 38.6$ larger than the Born self-energy in the bulk fluid, which is equal to $q^2/(8\pi\epsilon a)$. (Equation (5) can also be obtained by calculating the interaction of the charge on the surface of the spherical shell with itself, as was done in the second section of Ref. [16]). In the case of capacitive desalination, the energy barrier for an ion to enter the pore due to U can be overcome by the voltage difference between the bulk solution and the electrode if it exceeds the difference between U in the pore and U in the bulk solution divided by q , which is approximately

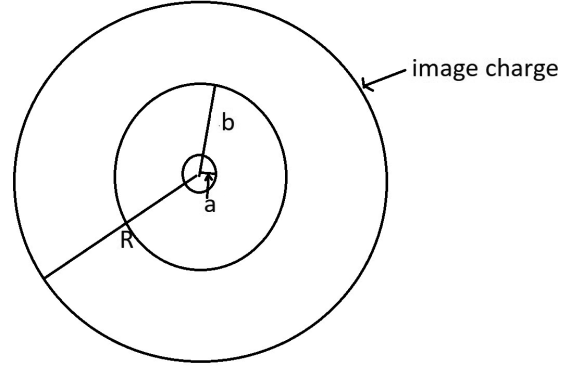


FIG. 2. Illustration of a charged ion of radius a at the center of a spherical cavity of radius b , which results in an image charge, which resides on a spherical shell of radius R .

equal to $2V$. Ionic screening of the electric field, however, can provide a sizable reduction in the self-energy. Reference [4] does not include the solvation energy.

Using Nordblom’s screening theory [16,17], which is valid for high ion concentrations, we have

$$E = \frac{Q}{4\pi\epsilon_{\text{perp}}r^2} \left(1 - \frac{r^3 - a^3}{h^3 - a^3}\right) \theta(r - a)\theta(h - r), \quad (6)$$

where $h \approx [3/(4\pi n_B) + a^3]^{1/3}$, with n_B equal to the number of ions per unit volume in the pore, and hence,

$$U = (1/2)\epsilon_{\text{perp}}(4\pi) \int_a^\infty r^2 dr E^2 \\ = \frac{q^2}{8\pi\epsilon_{\text{perp}}(h^3 - a^3)^2} \left(\frac{h^6}{a} + h^3 a^2 - \frac{9h^5 + a^5}{5}\right) \\ = \frac{q^2}{8\pi\epsilon_{\text{perp}}a} \Gamma, \quad (7)$$

where

$$\Gamma = \left(\frac{h^3}{a^3} - 1\right)^{-2} \left(\frac{h^6}{a^6} + \frac{h^3}{a^3} - 1.8\frac{h^5}{a^5} - 0.2\right). \quad (8)$$

Some values of Γ are given in Table I. The correlation hole approach to screening used in Ref. [4], appears to be equivalent to the approach used in Ref. [17] in the high ion density limit. The “correlation hole” referred to in Ref. [4] is identical to the screening charge sphere of radius h discussed above when $a \ll h$, but the maximum ion concentration in the data fit with the model presented in Ref. [4] of 60 mM ($3.61 \times 10^{25} \text{m}^{-3}$) is considerably smaller than the concentration at which one expects the Nordblom theory [17] is expected to be valid. Therefore, the screening length should be of the order of the Debye-Hückel screening length, which for this concentration is equal to 0.538 nm, and hence the argument used in Ref. [4] might still be qualitatively correct. On the basis of the values of Γ given in the table, the screening will not be sufficient to reduce the self-energy at the center of the pore by a sufficient amount to make it smaller than the self-energy in the bulk fluid. This implies that the ions would

TABLE I. Γ is given for several values of n_B , including $3.65 \times 10^{26} \text{ m}^{-3}$, the salt concentration of sea water and $3.65 \times 10^{27} \text{ m}^{-3}$, the salt concentration at the solubility limit of sodium chloride.

n_B	h/a for a Na^+ ion	Γ for a Na^+ ion	h/a for a Cl^- ion	Γ for a Cl^- ion
10^{26} m^{-3}	11.5	0.848	8.00	0.793
$3.65 \times 10^{26} \text{ m}^{-3}$	7.48	0.771	5.20	0.672
$2 \times 10^{27} \text{ m}^{-3}$	4.24	0.594	2.99	0.475
$3 \times 10^{27} \text{ m}^{-3}$	3.73	0.560	2.63	0.411
$3.65 \times 10^{27} \text{ m}^{-3}$	3.50	0.517	2.47	0.383

not be able to enter the pore, in the absence of an electrical potential difference due to an external source between the bulk solution and the pore.

If the center of the ion were within a distance a from the wall of the pore which is much less than b (assuming that $a \ll b$), the ion would “see” the surface of the pore as a plane to a good approximation, and hence, from Table III in Ref. [15] for the image potential resulting from a metallic planar surface, we obtain for an ion located at the wall

$$U_{\text{image}} \approx -1.3 \frac{q^2}{8\pi\epsilon_{\parallel}(b-d)} = -1.3 \frac{q^2}{8\pi\epsilon_{\parallel}a}, \quad (9)$$

where d is the distance of the center of the ion from the center of the pore for $\epsilon_{\parallel} = 81\epsilon_0$, $\epsilon_{\text{perp}} = 2.1\epsilon_0$. Of course, for ions lying against the wall there will be a van der Waals potential energy comparable and possibly larger than the image potential energy, which drops off rapidly when one moves a short distance from the wall. The image potential as a function of the distance from a flat wall is plotted in Fig. 3 as a function of its distance z from the wall below using Eq. (26) in Ref. [16]. Also included is a plot of $U_{\text{image}}(z=a)(a/z)$ (the lower plot). This shows that $U_{\text{image}}(z)$ is approximately inversely proportional to z .

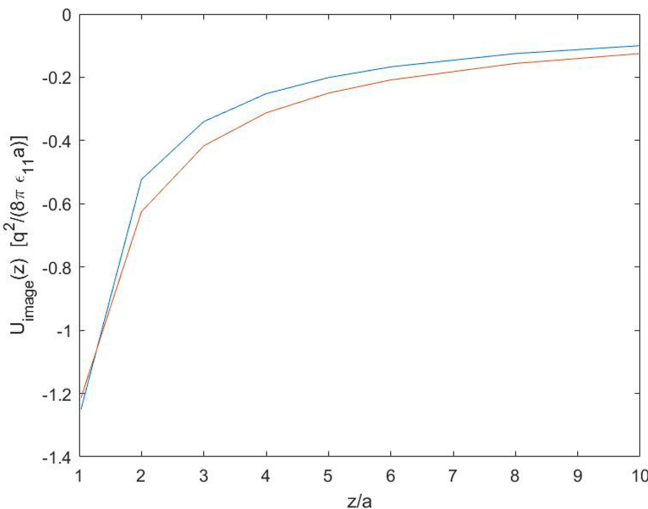


FIG. 3. The top curve is a plot of the image potential energy for a charged sphere of radius a as a function of the distance z of its center from a plane metallic wall. Lower curve is a plot of $U_{\text{image}}(z=a)(a/z)$ as a function of z .

Also, the self-energy near a plane wall (and hence near the wall of the spherical pore) from Table I in Ref. [16] is

$$U \approx 2.55 \frac{q^2}{8\pi\epsilon_{\parallel}a}. \quad (10)$$

An approximate calculation of the image potential for a point ion located away from the center of the pore, in the limit of small $\epsilon_{\text{perp}}/\epsilon_{\parallel}$, on the basis of a solution of Poisson’s equation for the tensor permittivity as an expansion in d/b , where d is the distance of the ion from the center of the pore, is given in Appendix A. The resulting image potential from Eqs. (A25) and (A26) is given by

$$U_{\text{image}} = -\frac{q^2}{4\pi\epsilon_{\text{perp}}b} \left[1 + A \left(\frac{\epsilon_{\text{perp}}}{\epsilon_{\parallel}} \right)^{1/2} \right], \quad (11)$$

where

$$A = \frac{b}{4\pi d} \sum_{\ell=1}^{\infty} [\ell(\ell+1)]^{1/2} v^{\ell(\ell+1)/2}, \quad (12)$$

where $v = (d/b)^{(\epsilon_{\parallel}/\epsilon_{\text{perp}})^{1/2}}$, which is given in Table II below. The results are also plotted in Fig. 4.

A plot of U_{image} versus d/b is given in Fig. 4.

The summation for A in Eq. (12) diverges as d/b approaches 1, indicating that this solution most likely breaks down as d/b approaches 1. The results for U_{image} cannot be used to obtain Eq. (9) because this calculation treated the ion as a point charge, which is correct only for ions that are a distance much larger than a from the wall. Since for relatively small values of d/b , A is smaller than 1, it appears that for ions that are far from the walls of the pore, U_{image} is of the order of the value given in Eq. (3). The image potential at the center of the pore, given by Eq. (3), is larger than it is near the

TABLE II. This table gives the parameter A as a function of d/b .

d/b	A
0.2	4.08×10^{-7}
0.7	0.0084
0.8	0.0321
0.9	0.180
0.95	0.792

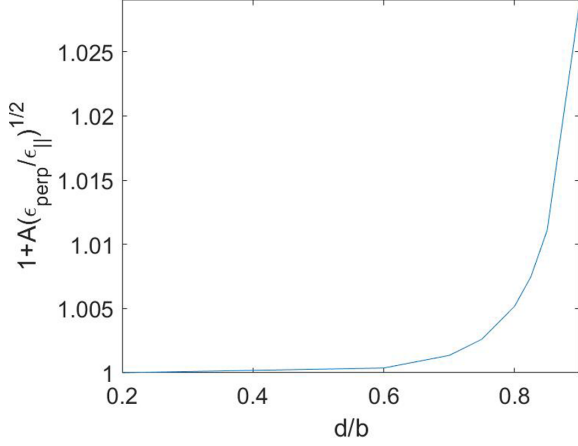


FIG. 4. Plot of the results of Table II for $-U_{\text{image}}$ for a circular pore in units of $q^2/(4\pi \epsilon_{\text{perp}}b)$ vs d/b .

wall if

$$\frac{2\epsilon_{\parallel}}{\epsilon_{\text{perp}}} \frac{a}{b} > 1.3. \quad (13)$$

On the basis of Eq. (13) we find that for $\epsilon_{\parallel} = 81\epsilon_0$, $\epsilon_{\text{perp}} = 2.1\epsilon_0$, if $a/b > 0.017$, the image potential at the center of a spherical pore is larger than it would be near a flat wall or between two parallel walls or near the wall of a spherical pore. The value of $U + U_{\text{image}}$ near the wall of the pore can be less than the value of U in the bulk fluid for the screening that occurs for an ion concentration of $2 \times 10^{27} \text{m}^{-3}$ or more [16]. This is possible because if the ion is at the wall and $a < h$, the screening due to the other ions does not eliminate the image potential energy of the ion. From Eqs. (3) and (5), however, it appears that $U + U_{\text{image}}$ inside and away from the walls of the pore will be larger than U in the bulk fluid. If $U + U_{\text{image}}$ inside the pore is less than U outside of the pore, ions can be absorbed in the pore even without a voltage difference between the regions inside and outside of a nanopore. In contrast, if $U + U_{\text{image}}$ inside the pore is larger than U outside of the pore, ions will only be absorbed by the pore if a voltage is applied between the electrodes greater than the difference between these energies divided by q . The treatment of nanopores in Ref. [18] considers the Born self-energy but does not include the tensor nature of the permittivity near a surface and the electrical image potential energy.

III. CYLINDRICAL PORES AND NANOTUBES

Let us now consider the image potential energy for a point charge to represent an ion a distance d from the axis of a metallic cylinder of radius b . The Coulomb potential in cylindrical coordinates is the solution to Poisson's equation:

$$\begin{aligned} \epsilon_{\text{perp}} \left(\frac{\partial^2 V}{\partial \rho^2} + \frac{1}{\rho} \frac{\partial V}{\partial \rho} \right) + \epsilon_{\parallel} \left(\frac{\partial^2 V}{\partial z^2} + \frac{1}{\rho^2} \frac{\partial^2 V}{\partial \phi^2} \right) \\ = -\frac{q}{\rho} \delta(\rho - d) \delta(\phi) \delta(z). \end{aligned} \quad (14)$$

The details of the solution of Eq. (14) are given in Appendix B by adapting the solution of Poisson's equation in Ref. [19]. We obtain for the image potential energy from

TABLE III. This table gives I' as a function of d/b .

d/b	I'
0.	0.280
0.2	0.283
0.3	0.287
0.5	0.300
0.7	0.329
0.9	0.446
0.95	0.599

Eq. (B26)

$$\begin{aligned} U_{\text{image}} = & -\frac{q^2}{8\pi \epsilon_{\text{perp}} b} \\ & \times \frac{4}{\pi} \sum_{m=0}^{\infty} \int_0^{\infty} dk' \frac{I_{m+1/2}(k'u^{1/2}d/b)^2 K_{m+1/2}(k'u^{1/2})}{I_{m+1/2}(k'u^{1/2})}, \end{aligned} \quad (15)$$

where $I_a(x)$, $K_a(x)$ are the modified Bessel functions of order a and where $k' = kb$. In Table III, the results for U_{image} are shown for $\epsilon_{\parallel} = 81\epsilon_0$, $\epsilon_{\text{perp}} = 2.1\epsilon_0$, where $I' = U_{\text{image}} (8\pi \epsilon_{\text{perp}} b/q^2)$.

The results in Table III are plotted in Fig. 5.

Again, as was the case for a spherical pore, U_{image} appears to diverge as d/b approaches 1, and since the ion was represented as a point charge in this calculation we cannot use it to make contact with Eq. (9). Since Ref. [20] shows that for tubes with radii of the order of a nanometer, ϵ_{\parallel} becomes larger than the bulk water permittivity of $81\epsilon_0$, let us calculate U_{image} for larger values of ϵ_{\parallel} . For example, for $d = 0$ and for $\epsilon_{\parallel} = 200\epsilon_0$, $U_{\text{image}} = 0.179 (q^2/8\pi \epsilon_{\text{perp}} b)$ and for $\epsilon_{\parallel} = 300\epsilon_0$, $U_{\text{image}} = 0.146 (q^2/8\pi \epsilon_{\text{perp}} b)$.

If we apply the results given in Table III to pores in porous electrodes, we conclude that for a pore with a radius of the order of a nanometer, the image potential is noticeably larger than the value used in Ref. [4]. It is difficult to evaluate U_{image} for d close to b , but since the wall should appear to the ion as being nearly flat, it should be well approximated by Eq. (9)

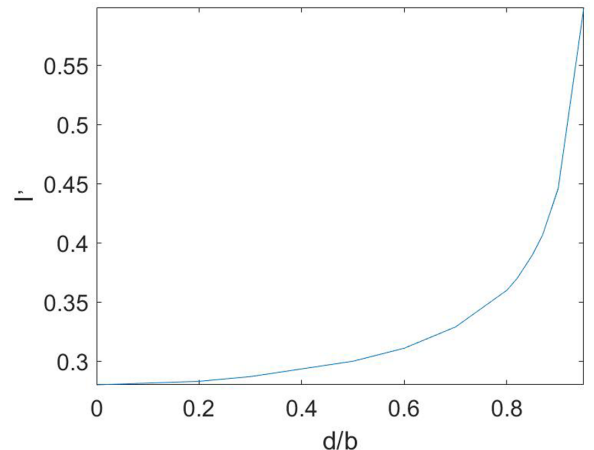


FIG. 5. Plot of the results of Table III for $I' = U_{\text{image}} (8\pi \epsilon_{\text{perp}} b/q^2)$.

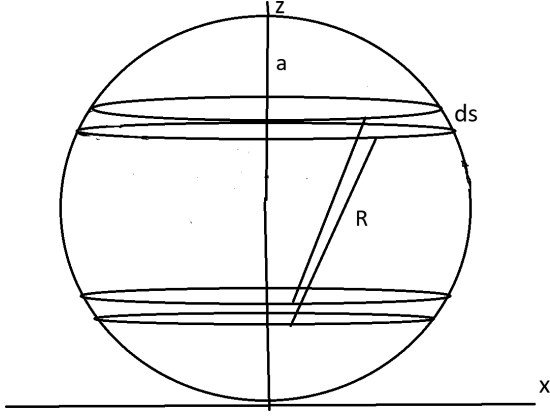


FIG. 6. Illustration of the calculation of the self-energy of an ion modeled as a charged spherical shell of radius a .

[16], for $b-d = a$, for an ion of radius a in contact with the wall. Inside the cylinder

$$U_{\text{image}} = -I' \frac{\varepsilon_{\parallel}}{\varepsilon_{\text{perp}}} \frac{a}{b} \frac{q^2}{8\pi\varepsilon_{\parallel}a}. \quad (16)$$

The self-energy can be calculated for an ion at the center of the cylinder as follows: Since from Eqs. (B19)–(B22) in Appendix B the Green function is given by

$$G(\vec{r} - \vec{r}') = \sum_{m=-\infty}^{\infty} e^{im(\phi-\phi')} \int_0^{\infty} dk \times J_{u^{1/2}m}(u^{1/2}k\rho) J_{u^{1/2}m}(u^{1/2}k\rho') e^{-k(z_{>} - z_{<})}, \quad (17)$$

with $u = \varepsilon_{\parallel}/\varepsilon_{\text{perp}}$, where for calculating the self-energy of a charged spherical shell model for the ion, we will set $\rho = (a^2 - z^2)^{1/2}$, $\rho' = (a^2 - z'^2)^{1/2}$ and $z_{>}$ is the larger of z and z' and $z_{<}$ is the smaller of z and z' . This is a Green function because $e^{-ik(z_{>} - z_{<})}$ is the Green function for the operator $d^2/dz^2 - k^2$. It is the solution of the equation

$$\left(\frac{\partial^2 G(\vec{r} - \vec{r}')}{\partial \rho^2} + \frac{1}{\rho} \frac{\partial G(\vec{r} - \vec{r}')}{\partial \rho} \right) + u \left(\frac{\partial^2 G(\vec{r} - \vec{r}')}{\partial z^2} + \frac{1}{\rho^2} \frac{\partial^2 G(\vec{r} - \vec{r}')}{\partial \phi^2} \right) = -\frac{1}{\varepsilon_{\text{perp}}\rho} \delta(\rho - d) \delta(\phi) \delta(z). \quad (18)$$

Then U is given by

$$U = \frac{1}{2} \frac{(\sigma a)^2}{4\pi\varepsilon_{\text{perp}}} \iint_{|\vec{r}|, |\vec{r}'|=a} d^3r d^3r' G(\vec{r} - \vec{r}') = \frac{1}{2} \frac{(\sigma a)^2}{4\pi\varepsilon_{\text{perp}}} \int_0^{2\pi} d\phi' \int_0^{2\pi} d\phi \sum_{m=-\infty}^{\infty} e^{im(\phi-\phi')} \times \int_{-a}^a dz' \int_{-a}^a dz \int_0^{\infty} dk \times J_{u^{1/2}m}(u^{1/2}k\rho) J_{u^{1/2}m}(u^{1/2}k\rho') e^{-k(z_{>} - z_{<})}, \quad (19)$$

as illustrated in Fig. 6, where $\rho = (a^2 - z^2)^{1/2}/a$, $\rho' = (a^2 - z'^2)^{1/2}/a$, since the element of area is given by $dA =$

$a \sin\theta d\theta a d\phi = a^2 dz d\phi$ (where θ is the azimuthal angle from spherical coordinates), and similarly for the primed quantities. Doing the integrals over ϕ and ϕ' and making the substitution $k' = u^{1/2}k$, we obtain

$$U = \frac{q^2}{32\pi u^{1/2} \varepsilon_{\text{perp}} a^2} \int_{-a}^a dz' \int_{-a}^a dz \int_0^{\infty} dk' \times J_0(k'\rho) J_0(k'\rho') e^{-k'u^{-1/2}(z_{>} - z_{<})}. \quad (20)$$

Doing the integral with $u = 81/2.1$ gives

$$U = \frac{q^2}{32\pi u^{1/2} \varepsilon_{\parallel} a^2} u \int_{-a}^a dz' \int_{-a}^a dz \int_0^{\infty} dk' \times J_0(k'\rho) J_0(k'\rho') e^{-k'u^{-1/2}(z_{>} - z_{<})} = \frac{u^{1/2} I}{4} \frac{q^2}{8\pi\varepsilon_{\parallel}a} = 8.86 \frac{q^2}{8\pi\varepsilon_{\parallel}a}, \quad (21)$$

where I is the above triple integral in Eq. (20). As is pointed out below Eq. (5), U is independent of b . This likely occurs because U only depends on the form of the tensor permittivity, which has been assumed to have the form that was used to calculate U above no matter how large we choose b to be. In reality, however, if the radius is large enough, the permittivity at the center of the tube will revert to its bulk water value [14]. If $\varepsilon_{\parallel} = \varepsilon_{\text{perp}} = \varepsilon$, $I = 4$ and hence U reduces to the Born value for a scalar permittivity of $U = q^2/(8\pi\varepsilon a)$, as expected. (Incidentally, the calculations of the self-energy and the image potential energy performed in Ref. [16] by an approximation valid to lowest order in $\varepsilon_{\text{perp}}/\varepsilon_{\parallel}$ can also be done by direct integration. Identical numerical results are obtained).

Let us now give some numerical illustrations of the effects of U_{image} and U for a solution of sodium chloride. Near the wall (a distance $d-a \ll b$), U_{image} is given by Eq. (9) and U is given by Eq. (10). We found that at the center of the tube U is given by Eq. (21). If $a = 0.167$ nm (i.e., for chlorine ions) and $b = 1$ nm, U_{image} at the center of the cylinder given by Eq. (16) is

$$U_{\text{image}} = -1.80 \frac{q^2}{8\pi\varepsilon_{\parallel}a}, \quad (22)$$

without considering the effect of screening on the image potential, (e.g., if the screening length h is larger than the distance of the ion from the cylinder's wall). Because of screening, the image potential energy is not likely to have a significant effect for ions located a distance greater than h from the cylinder's wall. Hence, even if the ionic concentration in the pore is close to the solubility limit (i.e., the ion concentration $3.65 \times 10^{27} \text{m}^{-3}$), which gives, using the screening factor Γ given in Table I for this concentration, the screened self-energy given by

$$U = 3.39 \frac{q^2}{8\pi\varepsilon_{\parallel}a}, \quad (23)$$

from Eqs. (7) and (21) and Table I. (Although the treatment of the effect of ionic screening used here of just multiplying the self-energy in the low concentration limit by Γ is strictly speaking only valid for spherical pores considered in the last section, the discussion of screening in Ref. [16] indicates that it should not be a bad approximation). Therefore, $U + U_{\text{image}}$

within the cylinder will still be greater than U in the bulk solution, which is equal to

$$U = \frac{q^2}{8\pi\epsilon_{\parallel}a}. \quad (24)$$

This will certainly be the case unless the ion is within a distance from the wall less than h . Near the walls, however, for an ion solution with concentration $3 \times 10^{27} \text{m}^{-3}$, $U + U_{\text{image}}$ will be less than the value of U in the bulk solution [16]. In the case of capacitive desalination, the solvation energy can be overcome by the external potential applied to the electrodes if the potential difference between the bulk solution and inside the pore or nanotube is greater than the difference between Eqs. (23) and (24) divided by q , which is equal to 0.127 V. If b were equal to 0.4 nm, however, $U_{\text{image}} = -5.07q^2/(8\pi\epsilon_{\parallel}a)$, for chloride ions, from Table III and Eq. (16), and hence $U + U_{\text{image}}$, even at a distance less than $d = h = 0.269$ nm from the walls of the pore or nanotube (corresponding to $d/b \approx 0.7$), using the value of U given by Eq. (23), will be less than the value of U in the bulk solution. Although for $b = 0.4$ nm the continuum approximation used in this paper is no longer valid (as the water forms one-dimensional chains) [21–28], this result suggests the importance of the image potential energy in allowing ions to occupy nanotubes or nanometer pores in electrodes.

Perhaps a more realistic, although crude, picture for an ion in a nanotube that is sufficiently narrow so that water enters the tube as a one-dimensional chain is the following: We assume that inside the tube, the permittivity is equal to ϵ_0 and the ion only interacts with the dipole moment of nearest-neighbor water molecules (assuming that the water dipole moments in the chain are completely disordered) with an interaction of the order of

$$U_e = -2 \frac{1}{4\pi\epsilon_0} \frac{qp}{r^2}, \quad (25)$$

where $p = 6.17 \times 10^{-30} \text{C m}$ is the dipole moment of a water molecule and $r^2 = a^2 - d^2/4$, where $d = p/e$. For $a = 0.167$ nm, we obtain $U_e = -1.25$ eV. Then, the solvation energy ΔU , which is the difference between the self-energy of the ion inside the tube and in the bulk solution, is

$$\Delta U = \frac{q^2}{8\pi\epsilon_0 a} \left(1 - \frac{\epsilon_0}{\epsilon}\right) + U_e = 3.05 \text{ eV}, \quad (26)$$

substituting $a = 1.67 \times 10^{-10} \text{m}$ and $\epsilon = 81\epsilon_0$. The image potential energy for an ion at the center of the tube found from Eq. (15) with $\epsilon_{\parallel} = \epsilon_{\text{perp}} = \epsilon_0$ is given by

$$U_{\text{image}} = -1.74 \frac{q^2}{8\pi\epsilon_0 a} = -7.50 \text{ eV}, \quad (27)$$

which means that

$$\Delta U + U_{\text{image}} = -4.45 \text{ eV}, \quad (28)$$

and hence, the total of the self-energy and the image potential inside the tube is lower than the self-energy outside of the tube.

So far, it has been assumed that the cylinder's wall is metallic. If the cylinder is taken to represent a single-wall nanotube,

it can be assumed to be a two-dimensional conductor if the electron mean-free path is smaller than the circumference. If not, it behaves as a 1D conductor (with conduction only along the z axis, the axis of the tube). Even if the tube behaves as a one-dimensional conductor, it will still be an equipotential, because of the following argument: The z component of the electric field is given, using Eq. (B24), by

$$E_z = -\frac{\partial V}{\partial z} = \frac{q}{2\pi^2\epsilon_{\text{perp}}} \sum_{m=-\infty}^{\infty} e^{im\phi} \times \int_0^{\infty} dk k \sin kz [I_{mu^{1/2}}(ku^{1/2}\rho_{<})K_{mu^{1/2}}(ku^{1/2}\rho_{>}) + A_m(k)I_{mu^{1/2}}(ku^{1/2}\rho)]. \quad (29)$$

If the tube is a one-dimensional conductor, when $\rho_{<} = d$, $\rho_{>} = \rho = b$,

$$0 = E_z = -\frac{\partial V}{\partial z} = \frac{q}{2\pi^2\epsilon_{\text{perp}}} \sum_{m=-\infty}^{\infty} e^{im\phi} \int_0^{\infty} dk k \sin kz [I_{mu^{1/2}}(ku^{1/2}d) \times K_{mu^{1/2}}(ku^{1/2}b) + A_m(k)I_{mu^{1/2}}(ku^{1/2}b)], \quad (30)$$

which gives the above value for $A_m(k)$. This means that

$$0 = E_{\phi} = -\frac{1}{\rho} \frac{\partial V}{\partial \phi} = -\frac{q}{2\pi^2\epsilon_{\text{perp}}} i \sum_{m=-\infty}^{\infty} m e^{im\phi} \int_0^{\infty} dk \cos kz \times [I_{mu^{1/2}}(ku^{1/2}\rho_{<})K_{mu^{1/2}}(ku^{1/2}\rho_{>}) + A_m(k)I_{mu^{1/2}}(ku^{1/2}\rho)] \quad (31)$$

on the surface of the cylinder where $\rho_{<} = d$, $\rho_{>} = \rho = b$, implying that the wall is an equipotential. In Misra and Blankshtein's simulation [29], graphene is assumed to be an perfect insulator, and thus, there is no electrical image potential energy. As long as the walls have any nonzero conductivity, however, when the ion is stationary, there will always be an image charge potential energy, as long as the one waits long enough for electrons in the wall to flow towards or away from the region in the wall opposite the ion. If the ion is moving parallel to the wall, however, it was shown in Appendix B of Ref. [30] that the image charge lags behind the ion by a distance parallel to the wall of

$$\Delta x \approx \frac{\epsilon_{\parallel} v}{\sigma_{2d}}, \quad (32)$$

where v is the velocity of the ion and σ_{2d} is the two dimensional electrical conductance of the wall. Thus, the ion will interact with the wall with an electrical image potential energy unless σ_{2d} is sufficiently small so that $\sigma_{2d}/\epsilon_{\parallel} \ll v$.

IV. TREATMENT OF THE INTERACTION OF AN ION WITH INSULATING WALLS

In Misra and Blankshtein's simulation [29], the interaction of an ion with the wall results from polarization of the individual carbon atoms, which was treated by a model in

which the polarization of the graphene is assumed to result from displacement of the electrons on a carbon atom with respect to its nucleus. In order to make contact with the polarization interaction in Misra and Blankenshtein's simulation [29], consider the following continuum model for the polarization interaction between a point ion of charge q and a 2D surface:

$$V_{\text{pol}}(\vec{r}) = \frac{1}{4\pi\epsilon_0} \sum_j \frac{\vec{p}_j \cdot (\vec{r} - \vec{r}_j)}{|\vec{r} - \vec{r}_j|^3} \approx \frac{1}{4\pi\epsilon_0} \int d^2r' \frac{\vec{\sigma}_p(\vec{r}') \cdot (\vec{r} - \vec{r}')}{|\vec{r} - \vec{r}'|^3}, \quad (33)$$

where the integral is over the surface of the cylinder and where $V_{\text{pol}}(\vec{r})$ is the potential at \vec{r} due to the dipole moment induced in the surface per unit area $\vec{\sigma}_p(\vec{r}')$, created by the electric field due to an ion located at the point \vec{r}_0 . Then, $\vec{\sigma}_p(\vec{r}')$ is given by

$$\vec{\sigma}_p(\vec{r}') = \frac{1}{4\pi\epsilon_0} \chi_p \frac{q(\vec{r}' - \vec{r}_0)}{|\vec{r}' - \vec{r}_0|^3}, \quad (34)$$

where χ_p is the susceptibility that gives the dipole moment per unit area induced by the ion's electric field. Then, substituting for $\vec{\sigma}_p(\vec{r}')$ in the above expression for $V_{\text{pol}}(\vec{r})$, evaluated at $\vec{r} = \vec{r}_0 = z_0\hat{z}$ gives the interaction between the ion and the polarization that it induces in the surface (which is the analog of U_{image} for an insulating surface) is given by

$$U_{\text{pol}} = qV_{\text{pol}}(\vec{r}_0) = \frac{q^2\chi_p}{(4\pi\epsilon_0)^2} \int dx dy \frac{1}{(z_0^2 + x^2 + y^2)^2} = \frac{q^2\chi_p}{16\pi\epsilon_0^2 z_0^2}. \quad (35)$$

It is proportional to z_0^{-2} , in contrast to the electrical image potential energy for a metallic surface, which is proportional to z_0^{-1} . When there is water present,

$$V_{\text{pol}}(\vec{r}) = \frac{1}{4\pi\epsilon_{\parallel}} \times \int d^2r' \frac{\sigma_{pz}(z-z') + (\epsilon_{\text{perp}}/\epsilon_{\parallel})[\sigma_{px}(x-x') + \sigma_{py}(y-y')]}{[(z-z')^2 + (\epsilon_{\text{perp}}/\epsilon_{\parallel})[(x-x')^2 + (y-y')^2]]^{3/2}} \quad (36)$$

and

$$\vec{\sigma}_p(\vec{r}') = \chi_p \frac{q}{4\pi\epsilon_{\parallel}} \frac{(z' - z_0)\hat{z} + (\epsilon_{\text{perp}}/\epsilon_{\parallel})(x'^2 + y'^2)}{[(z' - z_0)^2 + (\epsilon_{\text{perp}}/\epsilon_{\parallel})(x'^2 + y'^2)]^{3/2}}. \quad (37)$$

Substituting in the expression for $V_{\text{pol}}(\vec{r})$ at $\vec{r} = \vec{r}_0 = z_0\hat{z}$, we obtain

$$U_{\text{pol}} = qV_{\text{pol}}(\vec{r}_0) = \frac{\chi_p q^2}{(4\pi\epsilon_{\parallel})^2} 2\pi \int_0^{\infty} \frac{\rho' d\rho'}{[z_0^2 + (\epsilon_{\text{perp}}/\epsilon_{\parallel})\rho'^2]^2} \approx \frac{\chi_p q^2}{16\pi\epsilon_{\parallel}\epsilon_{\text{perp}}z_0^2}. \quad (38)$$

The susceptibility in mks units is given by

$$\chi_p = 4\pi\epsilon_0 n\alpha, \quad (39)$$

where n is the number of carbon atoms per unit area and α is the polarizability of a carbon atom [29] (which in cgs units has units of distance cubed), giving

$$U_{\text{pol}} = \frac{\epsilon_0 n\alpha q^2}{4\epsilon_{\parallel}\epsilon_{\text{perp}}z_0^2}. \quad (40)$$

Since $\epsilon_{\text{perp}} \approx \epsilon_0$ and $n\alpha$ is of the order of or a little smaller than a unit-cell dimension, the image potential energy in the polarization model is of the order of or a little smaller than the image potential energy for metallic surface. In other words it is reduced by a factor of $\epsilon_0/\epsilon_{\parallel}$ from its vacuum value.

For an ion at the center of a nonmetallic cylinder, the electrical potential produced by the ion at the origin is given in cylindrical coordinates by

$$V(\rho, z) = \frac{q}{4\pi\epsilon_{\text{perp}}[(\epsilon_{\parallel}/\epsilon_{\text{perp}})\rho^2 + z^2]^{1/2}}, \quad (41)$$

and hence,

$$\vec{E}(\rho, z) = \frac{q}{4\pi\epsilon_{\text{perp}}} \left[\frac{\rho(\epsilon_{\parallel}/\epsilon_{\text{perp}})\hat{\rho} + z\hat{z}}{[(\epsilon_{\parallel}/\epsilon_{\text{perp}})\rho^2 + z^2]^{3/2}} \right]. \quad (42)$$

Since $\vec{\sigma}_p(\vec{r}) = \chi_p \vec{E}(\vec{r})$ and

$$U_{\text{pol}} = 2\pi b q \int_{-\infty}^{\infty} dz \vec{\sigma}_p \cdot \vec{E}(\vec{r}), \quad (43)$$

$$U_{\text{pol}} = \frac{q^2\chi_p b}{8\pi\epsilon_{\text{perp}}^2} \int_{-\infty}^{\infty} dz \frac{b^2(\epsilon_{\parallel}/\epsilon_{\text{perp}})^2 + z^2}{[(\epsilon_{\parallel}/\epsilon_{\text{perp}})b^2 + z^2]^3} = \frac{q^2\chi_p}{8\pi\epsilon_{\text{perp}}^2 b^2} \int_{-\infty}^{\infty} d\bar{z} \frac{(\epsilon_{\parallel}/\epsilon_{\text{perp}})^2 + \bar{z}^2}{[(\epsilon_{\parallel}/\epsilon_{\text{perp}}) + \bar{z}^2]^3} = \frac{q^2\chi_p}{8\pi\epsilon_{\text{perp}}^2 b^2} \frac{[3(\epsilon_{\parallel}/\epsilon_{\text{perp}}) + 1]\pi}{8(\epsilon_{\parallel}/\epsilon_{\text{perp}})^{3/2}}, \quad (44)$$

where $\bar{z} = z/b$. For $\epsilon_{\parallel}/\epsilon_{\text{perp}} = 81/2.1$,

$$U_{\text{pol}} = 0.191 \frac{q^2\chi_p}{8\pi\epsilon_{\text{perp}}^2 b^2} = 0.095 \frac{q^2 n\epsilon_0 \alpha}{\epsilon_{\text{perp}}^2 b^2}, \quad (45)$$

using the above expression for χ_p , which makes it larger than the interaction with a flat insulating surface by a factor of $0.38\epsilon_{\parallel}/\epsilon_{\text{perp}}$ or a factor of 14.7 for the above values of the permittivity components. From Table III,

$$U_{\text{image}} = 0.28 \frac{q^2}{8\pi\epsilon_{\text{perp}} b}. \quad (46)$$

At the center of a metallic tube with the above values of the permittivity components, the ratio of the image potential energy for an insulating wall to that for a metallic wall is $8.52(\epsilon_0/\epsilon_{\text{perp}})(n\alpha/b)$. Since $n\alpha \approx a$, the ratio of the image potential for an insulating and for a metallic nanotube is of the order of a/b .

V. RELATIONSHIP OF SOME OF THE RESULTS PRESENTED HERE TO SOME EXPERIMENTS ON IONS IN NANOPORES IN ELECTRODES AND TO IONS IN NANOTUBES

In Ref. [4] a model based on the screened electrical image potential energy was used to fit experimental data on absorp-

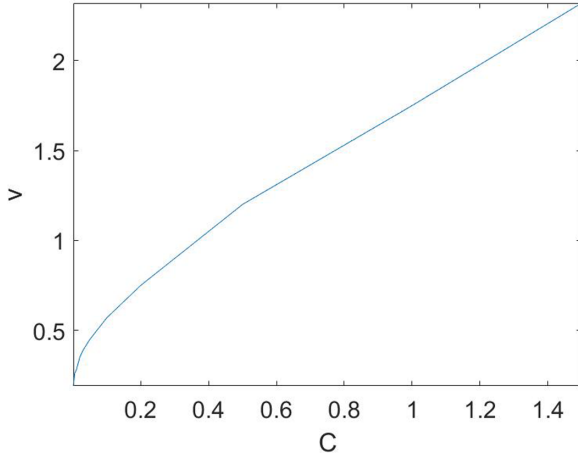


FIG. 7. Plot of a solution of Eq. (48) for v vs C .

tion of ions in nanopores in porous electrodes. In particular, Ref. [4] presents the following expression for the total concentration of ions (both positive and negative) in a pore based on Eqs. (6) and (12) in that reference:

$$c_{\text{ions,mi}} = 2c_{\infty} \cosh \Delta\phi_d e^{-\mu_{\text{att}}}, \quad (47)$$

where c_{∞} is the concentration of ions outside of a nanopore, $\Delta\phi_d$ is the electrical potential difference between inside the nanopore and outside of it divided by $k_B T$, and μ_{att} is the sum of all the interactions of the ion with the pore walls which are independent of the sign of the ion's charge divided by $k_B T$. In their model, the only contribution to μ_{att} is the electrical image potential with screening, which is argued to be inversely proportional to $c_{\text{ions,mi}}$. If we write it as $\mu_{\text{att}} = -f/c_{\text{ions,mi}}$, where f is a constant (equal to the ratio of the Bjerrum length and mean distance of the ion from the wall of the pore), and we set $v = c_{\text{ions,mi}}/f$, we can write the above expression for the mean ion concentration in a pore as

$$v = C e^{1/v}, \quad (48)$$

where $C = 2(c_{\infty}/f) \cosh(\Delta\phi_d)$ as plotted in Fig. 7. If we solve the above equation for v numerically, we obtain the following plot, which has the same form as Fig. 6 in Ref. [4]. As was discussed above, at the ion concentrations at which capacitive desalination takes place, Debye-Hückel screening should be more appropriate than the Nordblum method [17] used in Sec. II. Applying Debye-Hückel screening to the image potential obtained from Eqs. (2) and (3) at the middle of the pore, one obtains

$$U_{\text{image}} = -\frac{q^2}{4\pi\epsilon_{\text{perp}}b(1+Ka)} e^{-K(b-a)}, \quad (49)$$

where $K = (8\pi c_{\text{im,ions}} \ell_B)^{1/2}$. U_{image} in units of $q^2/(4\pi\epsilon_{\text{perp}}b)$ is plotted vs Ka below for $b = 2a$. See Fig. 8.

The self-energy, obtained by applying Debye-Hückel screening to Eqs. (4) and (5), is given by

$$\begin{aligned} U &= \frac{1}{2} \frac{\epsilon_{\text{perp}}(4\pi)}{(1+Ka)^2} \int_a^b r^2 dr \left[\frac{q}{(4\pi\epsilon_{\text{perp}})r^2} e^{-K(r-a)} \right]^2 \\ &= \frac{q^2}{8\pi\epsilon_{\text{perp}}a} \frac{Ka e^{2Ka}}{(1+Ka)^2} \int_{Ka}^{Kb} \frac{dx}{x^2} e^{-2x}, \end{aligned} \quad (50)$$

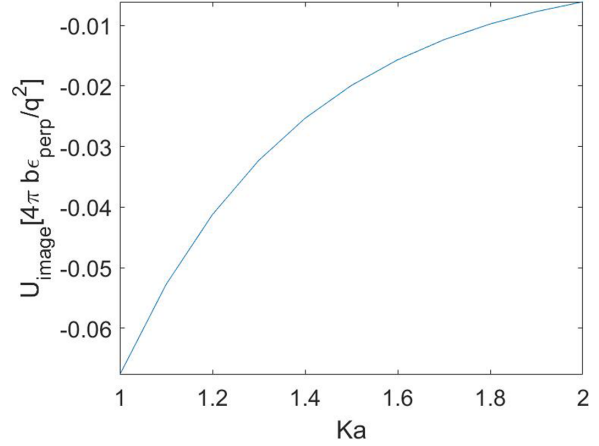


FIG. 8. Plot of Eq. (49) of U_{image} vs Ka for $b = 2a$.

where $x = Kr$. U in units of $q^2/(8\pi\epsilon_{\text{perp}}a)$ is plotted below versus Ka for $Kb = 2$ and $Kb = 10$ in Fig. 9.

We can see from the above figures for the image potential and the self-energy as a function of the ion concentration that the image potential energy is approximately proportional to $1/c_{\text{ions,mi}}$ (since $K \propto c_{\text{ions,mi}}^{1/2}$), whereas the self-energy is closer to being approximately proportional to $1/c_{\text{ions,mi}}^{1/2}$. Since the self-energy contribution to μ_{att} is positive, the exponential factor from the self-energy pushes the ion concentration in a pore to smaller values, unless $\Delta\phi_d$ is increased to compensate for this. To include both the image potential energy and the repulsive self-energy, we write the above equation to solve for v as

$$v = C e^{(1/v - g/v^{1/2})}, \quad (51)$$

where g is a constant and where $g/v^{1/2}$ represents the self-energy. (The exponential should contain the difference between this term and the self-energy outside the pore, which would be equal to the solvation energy, but since the self-energy outside is independent of $c_{\text{ions,mi}}$, it can be absorbed into C). This equation is solved for v versus C and plotted as a function of v .

Since the plot in Fig. 10 has the same approximate shape as the plot in Fig. 7, we see that even with the self-energy included, it should be possible to fit the data with this model. This is clearly correct if the image potential energy can become larger in magnitude than the self-energy at some point in the pore. Otherwise, the ions cannot enter the pore unless the applied potential exceeds the self-energy, as discussed above in Secs. II and III.

Recent experiments show that dissolved salt ions are able to flow through carbon nanotubes with a diameter smaller than a nanometer, contrary to previous molecular dynamics simulations [31], which predict that salt ions should not be able to enter such tubes because their solvation energy is much larger inside than outside the tube [32]. These results are explained by the existence of an attractive energy due to the polarization of the carbon atoms in the nanotube walls which counters the increase in the solvation energy when an ion enters the tube.

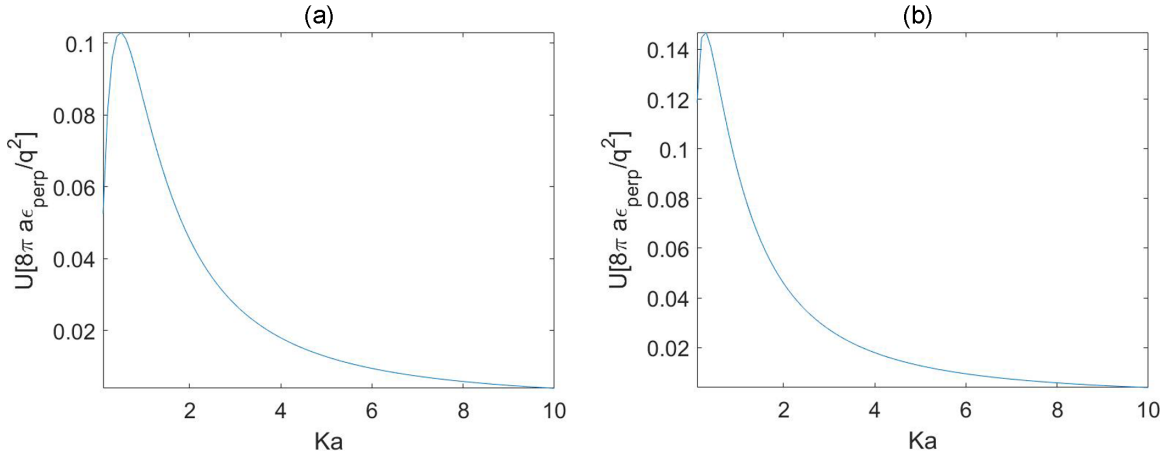


FIG. 9. Plot of U vs Ka from Eq. (50) for (a) $b = 2a$ and (b) $b = 10a$.

VI. CONCLUSIONS

It has been shown that electrical image potential energy can play an important role in allowing ions in an ionic solution to be absorbed by nanometer-scale pores in metallic electrodes, but it appears that it is only in pores of size less than a nanometer that the sum of the ion's solvation energy and its image potential energy within the pore is smaller than the ion's solvation energy in the bulk solution, which would allow the ions to reside in the pore. This is the case unless the potential difference between the bulk solution and the inside of the pore exceeds the difference between the solvation energy in the bulk solution and the sum of the solvation and image potential energy inside the pore, which is only 0.127 V. For a subnanometer-radius cylindrical pore or a nanotube, however, the sum of the electrical image potential energy and the Born self-energy of an ion is able to be lower than the self-energy of an ion in the bulk water, making it possible for ions to spontaneously enter the pore or nanotube. The Born expression for the self-energy is believed to be an overestimate [33–36]. Therefore, these conclusions can only be used to predict trends. In fact, for sodium ions, the solvation energy can be as much as a factor of 57% smaller than the

value given by the Born approximation [16,33]; for chloride ions, it is only reduced by a factor of 94%. This implies that positive ions will be more likely to be able to enter nanotubes and pores, because $U + U_{\text{image}}$ inside the tube or pore is more likely to be smaller than U outside the tube or pore. With the exception of motion of solutions in tubes or pores which are comparable in size to water molecules, there is good reason to believe that continuum theories of nanoscale fluids are valid at the nanoscale [37]. The polarization energy for insulating nanotubes (the analog of U_{image}) was shown to be comparable U_{image} to for nanometer-scale tubes, dominating for b not too much larger than a .

ACKNOWLEDGMENT

I wish to thank Alex Noy for discussions that I had with him about his unpublished work, which inspired some of the calculations in this paper.

APPENDIX A: IMAGE POTENTIAL ENERGY FOR A SPHERICAL PORE

Consider Poisson's equation in spherical coordinates [19],

$$\begin{aligned} \varepsilon_{\text{perp}} \frac{1}{r} \frac{\partial^2}{\partial r^2} (rV) + \varepsilon_{\parallel} \frac{1}{r^2 \sin \theta} \frac{\partial}{\partial \theta} \left(\sin \theta \frac{\partial V}{\partial \theta} \right) + \frac{\varepsilon_{\parallel}}{r^2 \sin^2 \theta} \frac{\partial^2 V}{\partial \phi^2} \\ = q \frac{1}{r^2} \delta(r - r') \delta(\cos \theta - \cos \theta') \delta(\phi - \phi'). \end{aligned} \quad (\text{A1})$$

If the ion is assumed to lie on the z axis, Poisson's equation has azimuthal symmetry. When a trial solution of the form $V(r, \theta) = r^{-1} R(r) P(\cos \theta) Q(\phi)$ is substituted in the associated homogeneous equation (i.e., Laplace's equation), we obtain

$$\begin{aligned} \frac{\varepsilon_{\text{perp}}}{R(r)} \frac{d^2 R(r)}{dr^2} + \frac{\varepsilon_{\parallel}}{r^2 \sin \theta P(\cos \theta)} \frac{d}{d\theta} \left(\sin \theta \frac{dP(\cos \theta)}{d\theta} \right) \\ + \frac{\varepsilon_{\parallel}}{r^2 \sin^2 \theta Q(\phi)} \frac{d^2 Q(\phi)}{d\phi^2} = 0. \end{aligned} \quad (\text{A2})$$

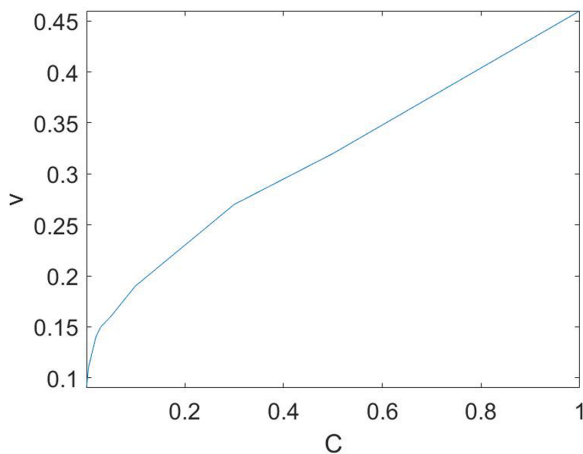


FIG. 10. Plot of a solution of Eq. (51), with $g = 2$, for v vs C .

Let us set

$$\frac{1}{\sin \theta P(\cos \theta)} \frac{d}{d\theta} \left(\sin \theta \frac{dP(\cos \theta)}{d\theta} \right) = -\ell(\ell + 1) + \frac{m^2}{\sin^2 \theta}, \quad (\text{A3})$$

and

$$\frac{1}{Q(\phi)} \frac{d^2 Q(\phi)}{d\phi^2} = -m^2, \quad (\text{A4})$$

with $0 < \ell < \infty$, $-\ell < m < \ell$, whose solutions are spherical harmonics $Y_\ell^m(\theta, \phi)$; we find that $R(r)$ is a solution to the equation

$$\frac{d^2 R(r)}{dr^2} = \frac{\varepsilon_{\parallel}}{\varepsilon_{\text{perp}}} \frac{\ell(\ell + 1)}{r^2}. \quad (\text{A5})$$

For $\ell \neq 0$ and large values of $\varepsilon_{\parallel}/\varepsilon_{\text{perp}}$, we can look for a solution of the form $R(r) = e^{u(r)}$. Substituting in the above equation we obtain

$$\left[\frac{d^2 u}{dr^2} + \left(\frac{du}{dr} \right)^2 \right] e^u = \left(\frac{\varepsilon_{\parallel}}{\varepsilon_{\text{perp}}} \right) \frac{\ell(\ell + 1)}{r^2} e^u. \quad (\text{A6})$$

Neglecting $d^2 u/dr^2$ gives solutions of the form

$$u = \pm \left(\frac{\varepsilon_{\parallel}}{\varepsilon_{\text{perp}}} \right)^{1/2} [\ell(\ell + 1)]^{1/2} \ln \frac{r}{b}, \quad (\text{A7})$$

where b is a constant. Since

$$\frac{d^2 u}{dr^2} = \mp \left(\frac{\varepsilon_{\parallel}}{\varepsilon_{\text{perp}}} \right)^{1/2} \frac{[\ell(\ell + 1)]^{1/2}}{r^2} \quad (\text{A8})$$

and

$$\left(\frac{du}{dr} \right)^2 = \frac{\varepsilon_{\parallel}}{\varepsilon_{\text{perp}}} \frac{\ell(\ell + 1)}{r^2}, \quad (\text{A9})$$

we are justified in neglecting the second derivative if $(\varepsilon_{\parallel}/\varepsilon_{\text{perp}})^{1/2}$ is sufficiently large. This approximation becomes better as ℓ increases. Since in our case $(\varepsilon_{\parallel}/\varepsilon_{\text{perp}})^{1/2}$ is only equal to 6.21, this solution is only a crude approximation. For $\ell = 0$, the solution for $R(r)/r$ has the form

$$\frac{R(r)}{r} = A + \frac{B}{r}, \quad (\text{A10})$$

where A and B are constants to be determined by boundary conditions. For $\ell > 0$,

$$\frac{R(r)}{r} = r^{-1} \left[A' \left(\frac{r}{b} \right)^{\alpha_\ell} + B' \left(\frac{b}{r} \right)^{\alpha_\ell} \right], \quad (\text{A11})$$

where A' and B' are constants and $\alpha_\ell = [(\varepsilon_{\parallel}/\varepsilon_{\text{perp}})\ell(\ell + 1)]^{1/2}$.

Following the derivation of the Green function in Ref. [19], we look for a Green function of the form

$$G(\vec{r}, \vec{r}') = \sum_{\ell=0}^{\infty} \sum_{m=-\ell}^{\ell} g_\ell(r, r') Y_\ell^m * (\theta', \phi') Y_\ell^m(\theta, \phi). \quad (\text{A12})$$

Substituting in Poisson equation above, we obtain the following equation for $g_\ell(r, r')$:

$$\begin{aligned} \frac{1}{r} \frac{d^2}{dr^2} [r g_\ell(r, r')] - \left(\frac{\varepsilon_{\parallel}}{\varepsilon_{\text{perp}}} \right) \frac{\ell(\ell + 1)}{r^2} g_\ell(r, r') \\ = \frac{1}{\varepsilon_{\text{perp}} r^2} \delta(r - r'). \end{aligned} \quad (\text{A13})$$

Integrating this equation over r from $r' - \delta$ to $r' + \delta$, where $\delta \ll 1$, we obtain

$$\frac{d}{dr} [r g_\ell(r, r')]_{r=r'+\delta} - \frac{d}{dr} [r g_\ell(r, r')]_{r=r'-\delta} = \frac{1}{\varepsilon_{\text{perp}} r'}. \quad (\text{A14})$$

Using the above approximate solution to Laplace's equation, we can write

$$g_\ell(r, r') = C \frac{1}{r_{<}} \left(\frac{r_{<}}{b} \right)^{\alpha_\ell} \frac{b}{r_{>}} \left[\left(\frac{r_{>}}{b} \right)^{\alpha_\ell} - \left(\frac{b}{r_{>}} \right)^{\alpha_\ell} \right], \quad (\text{A15})$$

for $\ell > 0$, where $r_{>}$ ($r_{<}$) is the larger (smaller) of r and r' . We have chosen b to represent the radius of the pore, where the potential must vanish. From the above continuity condition, we can write

$$\begin{aligned} \frac{d}{dr} [r g_\ell(r, r')]_{r=r'+\delta} - \frac{d}{dr} [r g_\ell(r, r')]_{r=r'-\delta} \\ = \frac{C}{r'} \left(\frac{r'}{b} \right)^{\alpha_\ell} \alpha_\ell \left[\left(\frac{r'}{b} \right)^{\alpha_\ell - 1} + \left(\frac{b}{r'} \right)^{\alpha_\ell + 1} \right] \\ - \frac{C}{r'} \alpha_\ell \left(\frac{r'}{b} \right)^{\alpha_\ell - 1} \left[\left(\frac{r'}{b} \right)^{\alpha_\ell} - \left(\frac{b}{r'} \right)^{\alpha_\ell} \right] = -\frac{1}{r'}, \end{aligned} \quad (\text{A16})$$

which gives

$$C = -\frac{1}{2\alpha_\ell \varepsilon_{\text{perp}}} \frac{r'}{b}. \quad (\text{A17})$$

Therefore, for $\ell \neq 0$

$$g_\ell(r, r') = -\frac{1}{2\alpha_\ell \varepsilon_{\text{perp}}} \left(\frac{r_{<}}{b} \right)^{\alpha_\ell} \left[\left(\frac{r_{>}}{b} \right)^{\alpha_\ell} - \left(\frac{b}{r_{>}} \right)^{\alpha_\ell} \right] \frac{r'}{r_{<} r_{>}}.$$

For $\ell = 0$,

$$g_0(r, r') = (1/2) \left(\frac{1}{r} - \frac{1}{b} \right). \quad (\text{A18})$$

Consider a uniformly charged sphere of radius a and total charge q . The charge density is given by

$$\rho(r') = \frac{q}{4\pi a^2} \delta(r' - a). \quad (\text{A19})$$

The potential is given by

$$V = \int d^3 r' G(r, r') \rho(r') = \frac{q}{4\pi \varepsilon_{\text{perp}}} \left(\frac{1}{r} - \frac{1}{b} \right), \quad (\text{A20})$$

our previous result. Since it is independent of a , it is also the result for a point charge at the origin. Now, let us consider the potential due to a point charge q at the point $z = d$ on the z axis. Then,

$$\rho(r') = \frac{q}{2\pi d^2} \delta(r' - d) \delta(\cos \theta' - 1), \quad (\text{A21})$$

which gives for the potential

$$V = \int d^3r G(\vec{r}, \vec{r}') \rho(r') = \frac{q}{2\pi \varepsilon_{\text{perp}}} \left[(1/2) \left(\frac{1}{r} - \frac{1}{b} \right) - \frac{1}{8\pi r} \sum_{\ell=1}^{\infty} [2\ell + 1] P_{\ell}(\cos \theta) \frac{1}{\alpha_{\ell}} \left(\frac{d}{b} \right)^{\alpha_{\ell}} \times \left[\left(\frac{r}{b} \right)^{\alpha_{\ell}} - \left(\frac{b}{r} \right)^{\alpha_{\ell}} \right] \right] \quad (\text{A22})$$

The image potential energy is then

$$U_{\text{image}} = -\frac{q^2}{4\pi \varepsilon_{\text{perp}}} \left[\frac{1}{b} + \frac{1}{4\pi d} \sum_{\ell=1}^{\infty} \ell(\ell + 1) \frac{1}{\alpha_{\ell}} \left(\frac{d}{b} \right)^{2\alpha_{\ell}} \right], \quad (\text{A23})$$

assuming that the $(b/d)^{\alpha_{\ell}}$ term in the last square bracket is part of the self-energy, since it gives a divergent contribution as $b/d \rightarrow \infty$. Also, the solution without a boundary only includes the $(b/d)^{\alpha_{\ell}}$ term. Then, U_{image} can also be

written as

$$U_{\text{image}} = -\frac{q^2}{4\pi \varepsilon_{\text{perp}}} \left[\frac{1}{b} + \frac{1}{4\pi d} \left(\frac{\varepsilon_{\text{perp}}}{\varepsilon_{\parallel}} \right)^{1/2} \times \sum_{\ell=1}^{\infty} [\ell(\ell + 1)]^{1/2} v^{[\ell(\ell+1)]^{1/2}} \right], \quad (\text{A24})$$

where $v = (d/b)^{(\varepsilon_{\parallel}/\varepsilon_{\text{perp}})^{1/2}}$. Then,

$$U_{\text{image}} = -\frac{q^2}{4\pi \varepsilon_{\text{perp}} b} \left[1 + A \left(\frac{\varepsilon_{\text{perp}}}{\varepsilon_{\parallel}} \right)^{1/2} \right], \quad (\text{A25})$$

where

$$A = \frac{b}{4\pi d} \sum_{\ell=1}^{\infty} [\ell(\ell + 1)]^{1/2} v^{[\ell(\ell+1)]^{1/2}}. \quad (\text{A26})$$

APPENDIX B: IMAGE POTENTIAL ENERGY FOR A CYLINDRICAL PORE OR NANOTUBE

In order to determine the Coulomb potential in cylindrical coordinates for an ion lying on the cylinder's axis, we must solve [19]

$$\varepsilon_{\text{perp}} \left(\frac{\partial^2 V}{\partial \rho^2} + \frac{1}{\rho} \frac{\partial V}{\partial \rho} \right) + \varepsilon_{\parallel} \left(\frac{\partial^2 V}{\partial z^2} \right) = -\frac{q}{\rho} \delta(\rho) \delta(z). \quad (\text{B1})$$

Making the substitution $\bar{\rho} = \rho/\varepsilon_{\text{perp}}^{1/2}$, $\bar{z} = z/\varepsilon_{\parallel}^{1/2}$, this equation becomes

$$\left(\frac{\partial^2 V}{\partial \bar{\rho}^2} + \frac{1}{\bar{\rho}} \frac{\partial V}{\partial \bar{\rho}} \right) + \left(\frac{\partial^2 V}{\partial \bar{z}^2} \right) = -\frac{1}{\varepsilon_{\parallel}^{1/2} \varepsilon_{\text{perp}} \bar{\rho}} \frac{q}{\bar{\rho}} \delta(\bar{\rho}) \delta(\bar{z}). \quad (\text{B2})$$

Since the solution to this equation without the factor $1/(\varepsilon_{\parallel}^{1/2} \varepsilon_{\text{perp}})$ is the Coulomb potential, the solution with this factor is

$$\frac{q}{4\pi \varepsilon_{\parallel}^{1/2} \varepsilon_{\text{perp}} (\bar{\rho}^2 + \bar{z}^2)^{1/2}}. \quad (\text{B3})$$

Then, the solution can be written as

$$\frac{q}{4\pi \varepsilon_{\text{perp}} [\rho^2 (\varepsilon_{\parallel}/\varepsilon_{\text{perp}}) + z^2]^{1/2}}. \quad (\text{B4})$$

The solution by separation of variables $V = R(\rho)Z(z)$ is as follows:

$$\frac{1}{R(\rho)} \left(\frac{d^2 R(\rho)}{d\rho^2} + \frac{1}{\rho} \frac{dR(\rho)}{d\rho} \right) + \frac{\varepsilon_{\parallel}}{\varepsilon_{\text{perp}}} \frac{1}{Z(z)} \frac{d^2 Z(z)}{dz^2} = 0. \quad (\text{B5})$$

Requiring that $Z(z)$ satisfy

$$\frac{d^2 Z(z)}{dz^2} = -k^2 Z(z), \quad (\text{B6})$$

where k^2 is a constant, we find that $R(\rho)$ satisfies

$$\frac{d^2 R(\rho)}{d\rho^2} + \frac{1}{\rho} \frac{dR(\rho)}{d\rho} - \frac{\varepsilon_{\parallel}}{\varepsilon_{\text{perp}}} k^2 R(\rho) = 0, \quad (\text{B7})$$

which is the equation for the modified Bessel function $I_0(uk\rho)$, where $u = (\varepsilon_{\parallel}/\varepsilon_{\text{perp}})^{1/2}$. Then, we can write

$$V(\rho, z) = \frac{q}{4\pi \varepsilon_{\text{perp}} [(\varepsilon_{\parallel}/\varepsilon_{\text{perp}})\rho^2 + z^2]^{1/2}} + (1/2) \int_{-\infty}^{\infty} dk A(k) e^{ikz} I_0(uk\rho). \quad (\text{B8})$$

We require that

$$0 = V(b, z) = \frac{q}{4\pi \varepsilon_{\text{perp}} [(\varepsilon_{\parallel}/\varepsilon_{\text{perp}})b^2 + z^2]^{1/2}} + (1/2) \int_{-\infty}^{\infty} dk A(k) e^{ikz} I_0(ukb), \quad (\text{B9})$$

where b is the radius of the pore. Then,

$$A(k)I_0(ukb) = -\frac{2q}{4\pi \varepsilon_{\text{perp}}} \frac{1}{2\pi} \int_{-\infty}^{\infty} dz \frac{e^{-ikz}}{[(\varepsilon_{\parallel}/\varepsilon_{\text{perp}})b^2 + z^2]^{1/2}}. \quad (\text{B10})$$

Therefore, the image potential energy is given by

$$U_{\text{image}} = -\frac{q^2}{8\pi \varepsilon_{\text{perp}}} \frac{4}{\pi} \int_0^{\infty} \frac{dk}{I_0(kub)} \int_0^{\infty} dz' \frac{\cos(kz')}{[u^2 b^2 + z'^2]^{1/2}}, \quad (\text{B11})$$

or setting $k' = kb$ and $z'' = z'/b$, we get

$$U_{\text{image}} = -\frac{q^2}{8\pi \varepsilon_{\text{perp}} b} \frac{4}{\pi} \int_0^{\infty} \frac{dk'}{I_0(k'u)} \int_0^{\infty} dz'' \frac{\cos(k'z'')}{[u^2 + z''^2]^{1/2}}. \quad (\text{B12})$$

Let us now consider a point charge which is a distance d off the axis (i.e., it is located at $x = d$). The potential due to the point charge satisfies

$$\varepsilon_{\text{perp}} \left(\frac{\partial^2 V}{\partial \rho^2} + \frac{1}{\rho} \frac{\partial V}{\partial \rho} \right) + \varepsilon_{\parallel} \left(\frac{\partial^2 V}{\partial z^2} + \frac{1}{\rho^2} \frac{\partial^2 V}{\partial \phi^2} \right) = -\frac{q}{\rho} \delta(\rho - d) \delta(\phi) \delta(z), \quad (\text{B13})$$

or

$$\left(\frac{\partial^2 V}{\partial \rho^2} + \frac{1}{\rho} \frac{\partial V}{\partial \rho} \right) + u \left(\frac{\partial^2 V}{\partial z^2} + \frac{1}{\rho^2} \frac{\partial^2 V}{\partial \phi^2} \right) = -\frac{q}{\varepsilon_{\text{perp}} \rho} \delta(\rho - d) \delta(\phi) \delta(z), \quad (\text{B14})$$

where $u = \varepsilon_{\parallel}/\varepsilon_{\text{perp}}$. The solution by separation of variables $V = R(\rho)Z(z)Q(\phi)$ is as follows:

$$\frac{1}{R(\rho)} \left(\frac{d^2 R(\rho)}{d\rho^2} + \frac{1}{\rho} \frac{dR(\rho)}{d\rho} \right) + u \left(\frac{1}{Z(z)} \frac{d^2 Z(z)}{dz^2} + \frac{1}{\rho^2} \frac{\partial^2 Q}{\partial \phi^2} \right) = 0. \quad (\text{B15})$$

Requiring that $Z(z)$ satisfy

$$\frac{d^2 Z(z)}{dz^2} = -k^2 Z(z), \quad (\text{B16})$$

where k^2 is a constant, and

$$\frac{d^2 Q}{d\phi^2} = -m^2 Q, \quad (\text{B17})$$

we find that $R(\rho)$ satisfies

$$\frac{d^2 R(\rho)}{d\rho^2} + \frac{1}{\rho} \frac{dR(\rho)}{d\rho} - u \left(k^2 + \frac{m^2}{\rho^2} \right) R(\rho) = 0, \quad (\text{B18})$$

whose solutions are $I_{mu^{1/2}}(u^{1/2}k)$, $K_{mu^{1/2}}(u^{1/2}k)$. Then, the Green function can be written as

$$G = \frac{1}{2\pi^2} \sum_{m=-\infty}^{\infty} \int_0^{\infty} dk e^{im(\phi-\phi')} \cos k(z-z') g_m(\rho, \rho'), \quad (\text{B19})$$

where $g_m(\rho, \rho')$ satisfies

$$\frac{1}{\rho} \frac{d}{d\rho} \left(\rho \frac{dg_m}{d\rho} \right) - u \left(k^2 + \frac{m^2}{\rho^2} \right) g_m = -\frac{1}{\rho} \delta(\rho - \rho'). \quad (\text{B20})$$

Integrating from $\rho = \rho' - \delta$ to $\rho = \rho' + \delta$, where $\delta \ll 1$, we get

$$\left. \frac{dg_m}{d\rho} \right|_{\rho=\rho'+\delta} - \left. \frac{dg_m}{d\rho} \right|_{\rho=\rho'-\delta} = -\frac{1}{\rho'}. \quad (\text{B21})$$

The solution is

$$g_m = C I_{mu^{1/2}}(x_{<}) K_{mu^{1/2}}(x_{>}), \quad (\text{B22})$$

where C is a constant, $x = ku^{1/2}\rho$, $\rho_<$ is the smaller of ρ , ρ' and $\rho_>$ is the larger of ρ , ρ' . Then, we have

$$C \left[I_{mu^{1/2}}(x') \frac{dK_{mu^{1/2}}(x)}{dx} - K_{mu^{1/2}}(x) \frac{dI_{mu^{1/2}}(x)}{dx} \right]_{x=x'} = -\frac{1}{x'}. \quad (\text{B23})$$

Since the bracketed expression (the Wronskian) is a constant for the equation satisfied by g_m , we can evaluate it at one point, such as the in the large- ρ limit, which gives a value of $-x'^{-1}$, and hence, we find that $C = 1$. Thus, from the above expression for the Green function we find that the potential due to a point charge located a distance d from the cylinder axis along the x axis (i.e., $\rho' = d$, $\phi' = 0$, $z' = 0$) is given by

$$V = \frac{q}{2\pi^2 \epsilon_{\text{perp}}} \sum_{m=-\infty}^{\infty} e^{im\phi} \int_0^{\infty} dk \cos kz [I_{mu^{1/2}}(ku^{1/2}\rho_<)K_{mu^{1/2}}(ku^{1/2}\rho_>) + A_m(k)I_{mu^{1/2}}(ku^{1/2}\rho)]. \quad (\text{B24})$$

The coefficient $A_m(k)$ is obtained by requiring that $V(\rho = b, z, \phi) = 0$, which gives

$$A_m(k) = -\frac{I_{mu^{1/2}}(ku^{1/2}d)K_{mu^{1/2}}(ku^{1/2}b)}{I_{mu^{1/2}}(ku^{1/2}b)}. \quad (\text{B25})$$

Inserting this expression for this coefficient and substituting $\rho = d$ and multiplying the second term in the square bracket by q we obtain for the image potential

$$U_{\text{image}} = -\frac{q^2}{8\pi \epsilon_{\text{perp}} b \pi} \sum_{m=0}^{\infty} \int_0^{\infty} dk' \frac{I_{mu^{1/2}}(k'u^{1/2}d/b)^2 K_{mu^{1/2}}(k'u^{1/2})}{I_{mu^{1/2}}(k'u^{1/2})}, \quad (\text{B26})$$

where $k' = kb$. In performing the integral over k' , the upper limit is chosen as the value of k' at which the integrand becomes negligibly small. Similarly, the upper limit on the summation over m was chosen as the value of m at which the summand becomes negligibly small.

-
- [1] Y. Salamat and C. Hidrovo, *Desalination* **438**, 34 (2018).
 [2] Y. Salamat, C. A. Rios Perez, and C. Hidrovo, *J. Energy Res. Technol.* **139**, 032003 (2017).
 [3] C. A. Rios Perez, O. N. Demirer, R. L. Clifton, R. M. Naylor, and C. H. Hidrovo, *J. Electrochem. Soc.* **160**, E13 (2013).
 [4] P. M. Biesheuvel, S. Porada, M. Levi, and M. Z. Bazant, *J. Solid State Electrochem.* **18**, 1365 (2014).
 [5] S. Porada, L. Borchardt, M. Oschatz, M. Bryjak, J. S. Atchison, K. J. Keesman, S. Kaskel, P. M. Biesheuvel, and V. Presser, *Energy Environ. Sci.* **6**, 3700 (2013).
 [6] A. Hemmatifar, M. Stadermann, and J. G. Santiago, *J. Phys. Chem. C* **119**, 24681 (2015).
 [7] R. Zhao, P. M. Biesheuvel, H. Miedema, H. Bruning, and A. van der Wal, *J. Phys. Chem Lett.* **113**, 205 (2010).
 [8] P. M. Biesheuvel and M. Z. Bazant, *Phys. Rev. E* **81**, 031502 (2010).
 [9] W. Tan, J. C. Stallard, C. Jo, M. F. L. De Volder, and N. A. Fleck, *J. Energy Storage* **41**, 102757 (2021).
 [10] J. Huang, B. G. Sumpter, and V. Meunier, *Angew. Chem. Int. Ed.* **47**, 520 (2008); C. O. Alvarez-Sanchez, J. A. Lasalde-Ramirez, E. O. Ortiz-Quiles, R. Masso-Ferret, and E. Nicolau, *Energy Sci. Eng.* **7**, 730 (2019).
 [11] A. VahidMohammadi, W. Liang, M. Mojtavavi, M. Wanunu, and M. Beidaghi, Energy storage materials (in press); B. E. Conway, *J. Electrochem. Soc.* **138**, 1539 (1991); S. Sarangapani, B. V. Tilak, and C.-P. Chen, *ibid.*, **143**, 3791 (1996).
 [12] A. S. Arico, P. Bruce, B. Scrosati, J.-M. Tarascon, and W. van Schalkwijk, *Nat. Mater.* **4**, 366 (2005); E. Frackowiak, *Phys. Chem. Chem. Phys.* **9**, 1774 (2007).
 [13] J. Yang, Y. Ding, C. Lian, S. Ying, and H. Liu, *Polymers* **12**, 722 (2020).
 [14] L. Fumagalli, A. Esfandiari, R. Fabregas, S. Hu, P. Ares, A. Janardannan, Q. Yang, B. Radha, T. Taniguchi, K. Watanabe, G. Gomila, K. S. Novoselov, and A. K. Geim, *Science* **360**, 1339 (2018).
 [15] J. B. Sokoloff, *Eur. Phys. J. E* **44**, 122 (2021).
 [16] M. Born, *Z. Phys.* **1**, 45 (1920).
 [17] S. Nordholm, *J. Chem. Phys. Lett.* **105**, 302 (1984).
 [18] T. Hennequin, M. Manghi, and J. Palmeri, *Phys. Rev. E* **104**, 044601(2021).
 [19] J. D. Jackson, *Classical Electrodynamics* (Wiley, New York, 1975).
 [20] P. Loche, C. Ayaz, A. Schlaich, Y. Uematsu, and R. R. Netz, *J. Phys. Chem. B* **123**, 10850 (2019).
 [21] X. Gao, T. Zhao, and Z. Li, *Phys. Fluids* **29**, 092003 (2017).
 [22] J. Köfinger, G. Hummer, and C. Dellago, *J. Chem. Phys.* **130**, 154110 (2009).
 [23] J. Köfinger and C. Dellago, *Phys. Rev. B* **82**, 205416 (2010).
 [24] J. Köfinger, G. Hummer, and C. Dellago, *Phys. Chem. Chem. Phys.* **13**, 15403 (2011).
 [25] R. H. Tunuguntla, R. Y. Henley, Y.-C. Yao, T. A. Pham, M. Wanunu, and A. Noy, *Science* **357**, 792 (2017).
 [26] G. Hummer, J. C. Rasaiah, and J. P. Noworyta, *Nature (London)* **414**, 188 (2001).
 [27] J. Köfinger, G. Hummer, and C. Dellago, *Proc. Natl Acad. Sci.* **105**, 10218 (2008).
 [28] J. Köfinger and C. Dellago, *Phys. Rev. Lett.* **103**, 080601 (2009).
 [29] R. P. Misra and D. Blankshtein, *Langmuir* **37**, 722 (2021).

- [30] J. B. Sokoloff, *Phys. Rev. E* **100**, 023112 (2019).
- [31] B. Corry, *J. Phys. Chem. B* **112**, 1427 (2008).
- [32] A. Noy (private communication).
- [33] W. M. Latimer, K. S. Pitzer, and C. M. Slansky, *J. Chem. Phys.* **7**, 108 (1939).
- [34] E. J. W. Verwey, *Recl. Trav. Chim. Pays-Bas* **61**, 127 (1942).
- [35] M. H. Abraham, J. Liszi, and L. Meszaros, *J. Chem. Phys.* **70**, 2491 (1979).
- [36] L. Beveridge and G. W. Schnuele, *J. Phys. Chem.* **79**, 2562 (1975).
- [37] L. Bocquet and E. Charlaix, *Chem. Soc. Rev.* **39**, 1073 (2010).